A new index of serial link manipulator performance combining dynamic manipulability and manipulating force ellisoids

Ryo Kurazume, *Member, IEEE,* and Tsutomu Hasegawa, *Member, IEEE,*

***Abstract*— The inertia matching ellipsoid (IME) is proposed as a new index of dynamic performance for serial link robotic manipulators. The IME integrates the existing dynamic manipulability and manipulating-force ellipsoids to achieve an accurate measure of the dynamic torque-force transmission efficiency between the joint torque and the force applied to a load held by an end-effecter. The dynamic manipulability and manipulating-force ellipsoids can both be derived from the IME as limiting forms with respect to the weight of the load. The effectiveness of the IME is demonstrated numerically through the selection of an optimal leg posture for jumping robots and optimal active stiffness control, and experimentally through application to a pick-up task using a commercial manipulator. The index is also extended theoretically to the case of a manipulator mounted on a free-flying satellite.**

***Index Terms*— Manipulators, Manipulator dynamics, Manipulability, Dynamic manipulability ellipsoid, Manipulating-force ellipsoid**

I. Introduction

A variety of indices have been proposed for evaluation of the performance of robot manipulators since the mid 1980s. The manipulability ellipsoid (ME) was introduced to evaluate the static performance of a robot manipulator as an index of the relationship between the angular velocities at each joint and the linear and angular velocity at the end-effecter of the manipulator [1]. The manipulating force ellipsoid (MFE) is a similar index that evaluates the static torque-force transmission from the joints to the end-effecter [2], while the dynamic manipulability ellipsoid (DME) is a measure of the dynamic performance of a robot manipulator based on the maximum acceleration of the end-effecter [3],[2],[4]. The compatibility index [5] and the condition number of the Jacobian matrix [6] were also proposed for determining the optimal posture for a particular task. The acceleration radius has also been proposed as performance measure, obtained as the minimum value of upper boundaries for the feasible acceleration of an end-effecter in the task space [7]. Asada et al. proposed a generalized inertial ellipsoid that allows the distributed mass system of the manipulator to be measured as a single-point mass system at the end-effecter [8].

These various indices provide a measure of the static and dynamic performance of the manipulator itself, specifically under no-load conditions. However, in some cases, it is important to be able to evaluate the performance when a load is applied at the end-effecter. For example, in the case that the load is limited to a discrete set of objects such as in pick-and-place tasks in assembly processes, an index that considers the effect of load would be convenient.

The concept of inertia matching is widely used in the analysis of actuator and gear systems, primarily for selection of the optimum gear ratio based on the transmission performance between the torque produced at the actuator and the torque applied to the load. This concept is sometimes referred to as ”impedance matching”. In this process, the performance of torque transmission is maximized by setting the optimal balance of inertial properties between the actuator system (including inertia of the rotor and shaft) and the load.

Alternatively, the Jacobian matrix can be used to measure the transformation between joint velocity and the velocity of the end-effecter of a robot manipulator. For an actuator and gear system, the input torque and velocity are transmitted to the output torque and velocity according to the gear ratio, as given by $\tau_{out} = \tau_{in}\xi$ or $\omega_{out} = \omega_{in}/\xi$. The torque and velocity produced at actuators of joints are transmitted to the torque, force and velocity at the end-effecter according to the posture of the manipulator. This transmission ratio can be described using the Jacobian matrix in a static configuration, that is, $\tau = J^T F_e$ or $v_e = J\dot{\phi}$. As the Jacobian matrix is analogous to the gear ratio of the actuator system mentioned above, the concept of inertia matching can be extended to the case of a serial-link manipulator as an index of the transmission efficiency between the torque produced at each joint and the force applied to the load at the end-effecter. This approach makes it possible to determine the optimal posture based directly on the transmission performance between the joint torque and the force applied to the load.

The concept of inertia matching for a serial link manipulator [9] is proposed in this paper as a new index of the dynamic performance of a manipulator. The proposed inertia matching ellipsoid (IME) characterizes the dynamic torque-force transmission efficiency between joint actuators and a load held by the end-effecter of a manipulator, encompassing a wide range of previous concepts. The DME and MFE, which are based on distinct concepts [2], are both derived from the IME as limiting forms regarding the weight of the load. This paper demonstrates the use of the IME through numerical examples, including the selection of an optimal leg posture for jumping robots, optimal active stiffness control, and extension to a manipulator mounted on a satellite in space. Experiments using

This paper was presented in part at the International Conference on Robotics and Automation, 2004.

R. Kurazume and T. Hasegawa are with the Graduate School of Information Science and Electrical Engineering, Kyushu University.

a typical serial link manipulator are also performed.

II. Inertia Matching for a Serial Link Manipulator

A. Inertia matching for an actuator

The basic premise of inertia matching for actuator systems is as follows. Let the moment of inertia of an actuator including the rotor and shaft be I_m, the moment of inertia of the load be I_l, the gear ratio be ξ, and the angular velocity of the load be ω_l. The equivalent torque produced by the actuator around the shaft, τ_m, can then be written as

$$\tau_m = \left(I_m + \frac{I_l}{\xi^2} \right) \xi \dot{\omega}_l \tag{1}$$

and the torque applied to the load, τ_l, can be given as

$$\tau_l = I_l \dot{\omega}_l \tag{2}$$

Therefore, the transmission efficiency between the torque produced at the actuator and the torque applied to the load can be defined as

$$\eta = \frac{\tau_l}{\tau_m} = \frac{I_l \dot{\omega}_l}{\left(I_m + \frac{I_l}{\xi^2} \right) \xi \dot{\omega}_l} \tag{3}$$

Thus, the optimal gear ratio that maximizes the transmission efficiency is determined by

$$\xi = \sqrt{\frac{I_l}{I_m}} \tag{4}$$

By choosing the optimal gear ratio by Eq. (4), a large acceleration of the load is produced with small output torque at the actuator. This is referred to as inertia matching for an actuator.

B. Inertia matching for a serial link manipulator

The concept of inertia matching for an actuator is extended to a serial link manipulator as follows. The motion equation for a serial link manipulator consisting of n joints and n links is written as

$$\tau = M(q)\ddot{q} + C(q, \dot{q}) + G(q) + J(q)^T F_e \tag{5}$$

where $\tau \in R^{n \times 1}$ is joint torque, $M(q) \in R^{n \times n}$ is the tensor of inertia for the manipulator in joint space, $C(q, \dot{q}) \in R^n$ contains the Coriolis and centrifugal forces, $G(q) \in R^n$ is the gravity force, $J(q) \in R^{m \times n}$ is the Jacobian matrix, and $F_e \in R^m$ is the external force and moment applied to the end-effecter. Here, m shows the degree of freedom of the end-effecter.

The motion equation for the load held at the end-effecter is given as

$$F_e = M_p \ddot{x} + M_p \mathbf{g} \tag{6}$$

where $\mathbf{g} = (g, 0)^T$, $\ddot{x} \in R^m$ is the acceleration of the end-effecter, $M_p \in R^{m \times m}$ is the inertia matrix of the load, and $g \in R^m$ is the acceleration of gravity. The acceleration of the end-effecter can thus be obtained as

$$\ddot{x} = J(q)\ddot{q} + \dot{J}(q)\dot{q} \tag{7}$$

Since the inertia matrix of the load M_p is a regular matrix, substituting Eqs. (6) and (7) into Eq. (5) leads to the following motion equation given in terms of the external force and moment:

$$\begin{aligned} \tau &= M(q)J(q)^\dagger M_p^{-1}(F_e - M_p\mathbf{g} - M_p\dot{J}(q)\dot{q}) \\ &\quad + C(q, \dot{q}) + G(q) + J(q)^T F_e \\ &= Q(q)(F_e - F_{bias}) \end{aligned} \tag{8}$$

where

$$\begin{aligned} F_{bias} &= W(J(q)^T + M(q)J(q)^\dagger M_p^{-1})^\dagger \\ &\quad [M(q)J(q)^\dagger(\mathbf{g} + \dot{J}(q)\dot{q}) - C(q, \dot{q}) - G(q)] \end{aligned} \tag{9}$$

$$Q(q) = J(q)^T + M(q)J(q)^\dagger M_p^{-1} \tag{10}$$

Here, $J(q)^\dagger \in R^{n \times m}$ is a pseudo inverse of the Jacobian matrix $J(q)$, and in the case that the Jacobian matrix is not a regular matrix can be obtained by

$$J(q)^\dagger = W^{-1}J^T(JW^{-1}J^T)^{-1} \tag{11}$$

where W is a weight matrix.

Equation (8) shows the relationship between the torque produced at the actuators and the force and moment applied to the load by the end-effecter. The coefficient matrix, $Q(q) \in R^{n \times m}$, indicates the torque-force transmission efficiency, and F_{bias} is a bias term related to current velocity and gravitation. Thus, singular value decomposition of this matrix $Q(q)$ affords the following equation:

$$Q(q) = U\Sigma V^T \tag{12}$$

where $\Sigma = diag(\sigma_1, \sigma_2, \cdots, \sigma_m) \in R^{m \times n}$, and $U \in R^{m \times m}$ and $V \in R^{n \times n}$ are orthogonal matrices. Therefore, the transmission efficiency between torque produced at each joint and the force and moment applied to the load by the end-effecter can be described by

$$w = \sigma_1^{-1} \cdot \sigma_2^{-1} \cdots \sigma_m^{-1} \tag{13}$$

In this paper, the value of w in Eq. (13) is defined as the inertia matching index, which indicates the degree of inertia matching for a serial link manipulator.

The inertia matching index defined by Eq. (13) is proportional to the hypervolume of the inertia matching ellipsoid, as defined in the next section. This is analogous to the relationship between the manipulability and the manipulability ellipsoid [1]. The proposed inertia matching index evaluates the torque-force transmission efficiency for all directions at an arbitrary position of the end-effecter.

Other possibilities for evaluating the magnitude of the matrix $Q(q)$ include, for example, $w = \sigma_1^{-1}$, $w = \sigma_1^{-1} + \sigma_2^{-1} + \cdots + \sigma_m^{-1}$, or $w = \frac{\sigma_1}{\sigma_m}$ (the condition number). In this paper, the product of the singular values of the matrix $Q(q)$ is adopted to maintain similarity with the manipulability or dynamic manipulability of existing indices.

If the Jacobian matrix $J(q)$ is not a square or regular matrix, the inertia matching index w varies depending on the choice of a pseudo inverse of the Jacobian matrix in

Eq. (11). This issue has been discussed for other indexes. For example, Chiacchio[10] proposed a new definition of a dynamic manipulability ellipsoid for a redundant manipulator by setting $W = M^T L^{-2} M$ (L is defined in Eq. 16). This is quite interesting since it may be possible to improve the inertia matching index for a redundant manipulator through appropriate choice of a torque distribution for redundant joints. However, further discussion about this issue is beyond the scope of this paper.

The proposed inertia matching index thus indicates the efficiency of torque-force transmission between the actuators at each joint and the load held at the end-effecter of the manipulator. This concept is illustrated more clearly by the inertia matching ellipsoid, which is introduced in the following section.

C. Inertia matching ellipsoid

The torque limits at each actuator in the serial link manipulator are assumed to be symmetrical, that is,

$$-\tau_i^{limit} \leq \tau_i \leq \tau_i^{limit} \tag{14}$$

Using the conversion matrix L,

$$L = diag(\tau_1^{limit}, \tau_2^{limit}, \cdots, \tau_n^{limit}) \tag{15}$$

the normalized joint torque $\tilde{\tau}$ can be obtained as

$$\tilde{\tau} = L^{-1}\tau \tag{16}$$

Therefore, when a normalized torque with magnitude of 1 is produced, the force and moment applied to the load are derived from

$$\tilde{\tau}^T \tilde{\tau} \leq 1 \tag{17}$$

as

$$(F_e - F_{bias})^T Q^T L^{-2} Q (F_e - F_{bias}) \leq 1 \tag{18}$$

This equation describes the ellipsoid of force and moment transmitted from joints to the load, that is, the inertia matching ellipsoid (IME).

D. Features of the IME

The IME defined by Eq. (18) coincides with the dynamic manipulability ellipsoid in the case that $M_p \to 0$, and the manipulating force ellipsoid in the case that $M_p \to \infty$.

To show this, we first assume $M_p \to 0$. Then, since $F_e = 0$ from Eq. (6), Eq. (8) can be rewritten as

$$\begin{aligned} \tau &= M(q)J(q)^\dagger(\ddot{x} - \dot{J}(q)\dot{q}) + C(q,\dot{q}) + G(q) \\ &= M(q)J(q)^\dagger(\ddot{x} - \ddot{x}_{bias}) \end{aligned} \tag{19}$$

Thus, Eq. (18) becomes

$$(\ddot{x} - \ddot{x}_{bias})^T (M(q)J(q)^\dagger)^T L^{-2} (M(q)J(q)^\dagger)(\ddot{x} - \ddot{x}_{bias}) \leq 1 \tag{20}$$

This equation is the definition of the DME.

For $M_p \to \infty$, we consider a stationary state ($\dot{x} = \ddot{x} = 0$) and ignore the effect of gravity. In this case, Eq. (18) can be revised as

$$F_e^T J(q) L^{-2} J(q)^T F_e \leq 1 \tag{21}$$

This equation describes the MFE.

Consequently, the IME is considered to have intermediate features between those of the DME and MFE, and both the DME and MFE can be derived as limiting forms in terms of the weight of the load. Koppe also integrated the DME and MFE for a particular task [2], but only considered the selection of indices individually in the task space. In contrast, the proposed IME includes both the DME and MFE as end points of a continuum related to the weight of the load.

E. Extension to mass-spring-damper model

When the load is supported by a spring and a damper, the following motion equation should be used for the load held at the end-effecter instead of Eq. (6)[11]:

$$F_e = M_p\ddot{x} + C_p\dot{x} + K_p\Delta x + M_p\mathbf{g} \tag{22}$$

In this model, the spring and damping characteristics at the contact point x are also considered. The proposed IME takes into account these contact conditions, which cannot be handled by the DME. Taking these additional effects into consideration, Eqs. (8), (9), and (10) can be rewritten as follows.

$$\tau = Q(q)(F_e - F'_{bias}) \tag{23}$$

$$\begin{aligned} F'_{bias} &= (J(q)^T + M(q)J(q)^\dagger M_p^{-1})^\dagger \\ &\quad [M(q)J(q)^\dagger(\mathbf{g} + M_p^{-1}C_p\dot{x} + M_p^{-1}K_p\Delta x \\ &\quad + \dot{J}(q)\dot{q}) - C(q,\dot{q}) - G(q)] \end{aligned} \tag{24}$$

$$Q(q) = J(q)^T + M(q)J(q)^\dagger M_p^{-1} \tag{25}$$

Equation (24) shows that the spring and damping characteristics emerge in the bias term F'_{bias}.

III. Numerical examples

A. Inertia matching index for an industrial manipulator

Figure 1 illustrates an example of the inertia matching index for a typical serial link manipulator, PA-10 (Mitsubishi Heavy Industry, Fig. 1). The inertia matching index is calculated on the $x - z$ plane as follows.

$$w = \sigma_x^{-1}\sigma_z^{-1} \tag{26}$$

The weight of the manipulator and the load are set at 32 and 5 kg in this example, respectively. In Fig. 1, the inertia matching index is large in the shaded region, indicating that the joint torque is transmitted to the load most efficiently when the manipulator is operated in this region.

Inertia matching for an actuator system provides the optimal gear ratio that maximizes the torque transmission efficiency, as calculated by Eq. (4). In the inertia matching scheme for a manipulator system proposed in this paper, the coefficient matrix Q is determined so as to maximize the inertia matching index defined by Eq. (13). However, as shown in Eq. (10), Q is a nonlinear function of joint angles or the weight of the load. Therefore, it is almost impossible to derive the Jacobian matrix that gives the optimal matrix Q analytically. Consequently, a workspace in which the inertia matching index is large should be registered in advance for various loads (Fig. 1). Then,

by operating the manipulator in this workspace during actual tasks, the joint torque should be transmitted efficiently (i.e., high acceleration/deceleration) to the load in all operations.

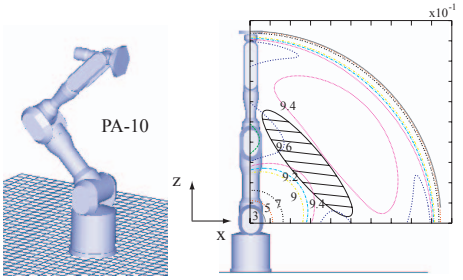

Fig. 1. Example of inertia matching for PA-10 manipulator

B. Design of optimal leg structure for jumping robots

Determination of the optimal leg posture for a two-link jumping robot is presented as a numerical example of the proposed inertia matching index.

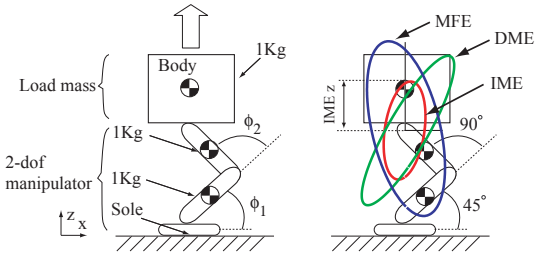

Fig. 2. Inertia matching ellipsoid for jumping robot

Let the length and the mass of each leg be 1 m and 1 kg, and the joint angles be ϕ_1 and ϕ_2, respectively. Figure 2 depicts the IME, DME, and MFE for a body mass of 1 kg with $\phi_1 = 45°$, $\phi_2 = 90°$, and the maximum torque limit τ^{limit} set at 10 Nm. The IME and MFE are given in units of N, while the DME is given in m^2/s.

Figure 2 shows that the IME is smaller than the MFE since it includes the torque consumption required to drive the mass of the manipulator itself. Moreover, the axis corresponding to the highest torque-force transmission efficiency is intermediate between those of the DME and the MFE. Thus, the IME has intermediate shape features compared to these ellipsoids.

The feasible output force in the z direction is compared between several initial postures by simulation. It is assumed that the sole is always placed under the center of the body, that is, $\phi_2 = \pi - 2\phi_1$. Figure 3 shows the values of the IME and DME in the z direction for several initial postures. The IME indicates a peak transmission efficiency at $\phi_1 = 54$ deg. In contrast, the DME decreases monotonically since it neglects the body mass. Figures 4 and 5 show the same indices for 4 different leg postures. For straightening of the legs, the width of the DME in the z direction decreases monotonically, while the width of the IME first increases then decreases.

The peak value indicated by the IME corresponds to the optimal posture in terms of torque-force transmission efficiency. Thus, using this posture, it is possible to apply a larger force to the body even if the same joint torque is produced. Since the jumping height is determined by the time integral of the force applied to the body, the proposed IME indicates the performance of the link structure of the jumping robot more accurately than conventional indices such as the DME or MFE.

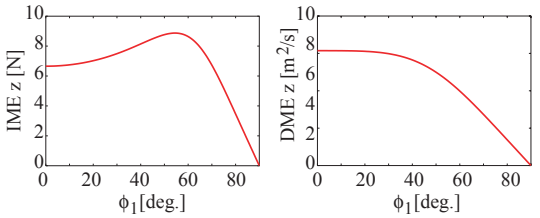

Fig. 3. Vertical force and acceleration derived from IME and DME

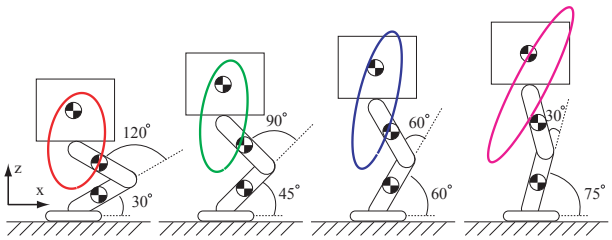

Fig. 4. IME for various leg postures

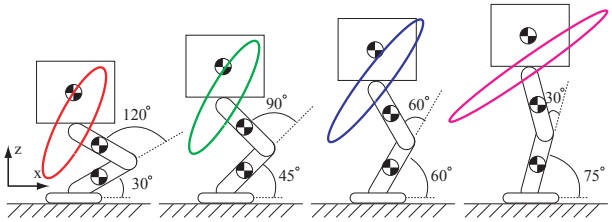

Fig. 5. DME for various leg postures

Jumping simulations for a two-link jumping robot were performed using the OpenHRP dynamic simulator. The length and mass of links were set that as shown in Fig. 2. A torque of 300 Nm was applied to joint 2 in the period 0–0.1 s, after which the joint was fixed. The maximum jumping height, given by the distance from the height at which the sole leaves the ground, is depicted in Fig. 6 for various leg postures. The maximum jumping height reaches a peak at $\phi_1 = 50°$, and decreases rapidly if ϕ_1 increases. These results are very much in agreement with the predicted by the proposed IME, as shown in Fig. 3.

C. Determination of optimal servo stiffness in active stiffness control for a serial link manipulator

The IME, DME, and MFE for the PA-10 serial link manipulator are shown in Fig.7. The PA-10 consists of 7 joints, including a rotational axis around an approach vector at the end-effecter. However, in this example, the terminal joint is omitted and the device simplified as a 6 degree of freedom (DOF) manipulator. The total weight of the PA-10 is 32 kg,

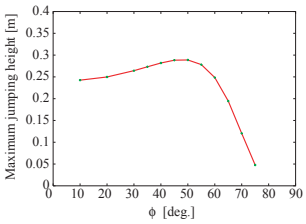

Fig. 6. Maximum jumping height for various leg postures

and the load grasped by the end-effecter is a cubic object in this case with a width of 0.1 m and weight of 1 kg. The maximum joint torque is determined according to the specification sheet.

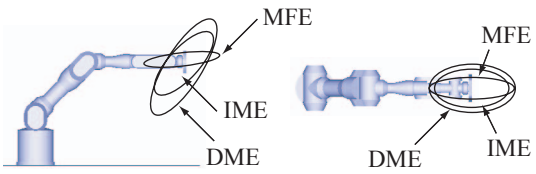

Fig. 7. Comparison of IME, DME, and MFE indices for the PA-10 as a 6 DOF manipulator

The IMEs for various load weights are illustrated in Fig. 8. The IME becomes small in the case of light loads, in which

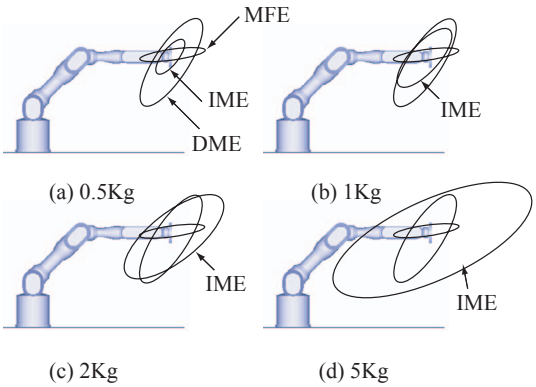

Fig. 8. Calculated IME for various load weights

case the majority of the produced joint torque is consumed by the motion of the manipulator itself. For heavy loads, however, the IME becomes large because most joint torque is transmitted to the load.

Active stiffness control [12] was proposed in the 1980s to realize impedance behavior of a manipulator based on the servo stiffness at each joint. However, the original active stiffness control does not consider the weight of either the load or the manipulator. Taking both weights into consideration, the optimal servo stiffness required to realize the desired impedance characteristics of the load in active stiffness control can be determined using the proposed IME as

$$\begin{aligned} \tau &= QSJ\delta q + QCJ\dot{q} - QF_{bias} \\ &= K\delta q + D\dot{q} + \tau_{bias} \end{aligned} \tag{27}$$

where S and C are the desired stiffness and viscosity at the end-effecter. Thus, by choosing the servo stiffness and the viscosity term as

$$K = QSJ \tag{28}$$
$$D = QCJ \tag{29}$$

the impedance characteristics are obtained as follows.

$$M_p\ddot{x} + C\dot{x} + S\Delta x = 0 \tag{30}$$

Equation (27) is used to determine the servo stiffness and viscosity term that realize the desired impedance characteristics according to the posture of the manipulator and the weight of the load. In conventional stiffness control, the servo stiffness is fixed, even if the weight of the load changes. In the proposed active stiffness control, the servo stiffness and viscosity term are calculated in advance for various load weights or manipulator postures. Then, by selecting appropriate gains according to the situation, the desired impedance characteristics can be realized more precisely than by the conventional approach, which does not consider the weight of the load.

D. Extension to a free-flying robot manipulator

The motion of a manipulator mounted on a free-flying satellite in space causes the satellite itself to undergo motion due to reactive force [13], [14]. Therefore, the mass of the manipulator affects the operational efficiency more severely than in the case of a ground-mounted manipulator. The proposed IME is extended here to such a situation.

Consider a free-flying robot with n joints and $n+1$ links, where the mass and tensor of inertia for each link are given by m_i and I_i, respectively. The linear and angular momenta around the center of gravity of the robot $N_g = (P_g, L_g)^T$ are then given by

$$N_g = MV_g \tag{31}$$

where $M = diag(wI_3, I_g)$, $w = \sum m_i$, $I_g = \sum I_i + m_i\tilde{r}_{gi}\tilde{r}_{gi}$, $V_g = (v_g, \omega_g)^T$, r_{gi} is a vector from the total center of gravity to the center of gravity of the link i, and $\tilde{r}$ is a skew-symmetric matrix. By differentiating Eq. (31), we obtain

$$\dot{N}_g = M\dot{V}_g + C_g \tag{32}$$

where $C_g = (0, \omega_g \times I_g\omega_g)^T$. The relationship between the force around the center of gravity and the force applied to the end-effecter is given by

$$F_g = -R_h^T f_h \tag{33}$$

where $F_g = \dot{N}_g$, $F_h = -(f_h, n_h)^T$ is the force and moment applied to the load by the end-effecter, and R_h^T is a matrix given by

$$R_h^T = \begin{pmatrix} I_3 & 0 \\ \tilde{r}_{gh} & I_3 \end{pmatrix} \tag{34}$$

Therefore, from Eqs. (32) and (33), the following equation can be obtained:

$$M\dot{V}_g + C_g = -R_h^T F_h \tag{35}$$

Using the generalized Jacobian matrix, J^*, for the free-flying robot proposed by Yoshida et al. [13], the following equation describing the relationship between the velocity of

the end-effecter, the center of gravity, and the angular velocity at each joint also holds:

$$V_h = J^*\dot{\phi} + R_h V_g \tag{36}$$

By solving Eq. (35) for F_h and substituting the derivative of Eq. (36), we obtain

$$F_h = -R_h^{-T} M R_h^{-1} \dot{V}_h + R_h^{-T} M R_h^{-1} J \ddot{\phi} \tag{37}$$

Here, only the stationary state is considered, and the squared velocity term is ignored for simplicity.

In the case that a load with an inertia matrix W is held at the end-effecter, the force applied to the load is given by

$$F_h = W \dot{V}_h \tag{38}$$

From Eqs. (37) and (38), the acceleration of the end-effecter is then given by

$$\begin{aligned} \dot{V}_h &= (R_h^{-T} M R_h^{-1} + W)^{-1} R_h^{-T} M R_h^{-1} J^* \ddot{\phi} \\ &= \Omega J^* \ddot{\phi} \end{aligned} \tag{39}$$

Thus, the force applied to the load in Eq. (38) can be revised as

$$F_h = W \Omega J^* \ddot{\phi} \tag{40}$$

where $\Omega = (R_h^{-T} M R_h^{-1} + W)^{-1} R_h^{-T} M R_h^{-1}$.

In general, the motion equation for a free-flying robot is given by

$$\tau = H^* \ddot{\phi} + C_g + J^{*T} F_h \tag{41}$$

where H^* is the tensor of inertia for the free-flying robot in joint space. By substituting Eq. (40) into Eq. (41), we obtain

$$\tau = (J^{*T} + H^* J^{*-1} \Omega^{-1} W^{-1}) F_h \tag{42}$$

This equation describes the joint torque required to accelerate the load (with inertia tensor W) at acceleration $\dot{V}_h$, as given by Eq. (39). Thus, Eq. (42) is an extension of the inertia matching scheme for serial link manipulators as defined by Eq. (8) to free-flying robots.

Comparing Eq. (42) with Eq. (8) in the case fo $\mathbf{g}$ and $\dot{q}$ equal to zero, the following correlations can be made.

$$J \rightarrow J^* \tag{43}$$

$$M_p \rightarrow W\Omega \tag{44}$$

Since Ω is a function of the joint angles, the effect of the load W at the end-effecter can be converted to the imaginary load $W\Omega$ for the free-flying robot. This imaginary weight will change according to the robot's posture. For example, consider a task that involves catching a failed satellite using a free-flying robot in space. By setting the optimal posture of the manipulator for catching the satellite, the weight of the satellite can be converted to $W\Omega$, allowing the torque required to catch the satellite to be reduced, along with the energy consumption. Conversely, for the release of a satellite into orbit, a large releasing force can be applied to the satellite with only a small joint torque by choosing the optimal posture of the manipulator.

IV. Experiments

The inertia matching index was also measured experimentally for the PA-10 manipulator. In the experiment, a heavy load was attached to the end-effecter, and the joint torque and force transmitted to the load was measured using a force sensor. Figure 9 shows the manipulator, load, and force sensor (BL Autotec) attached at the wrist of the robot. The weight of the manipulator and the load were 32 and 4.5 kg, respectively. The posture of the manipulator was determined such that the wrist was positioned just above the axis of the first joint, as shown in Fig. 10. Here, the angle of the second joint is defined as θ, as shown in Fig. 9. The output of the force sensor and the joint torque were measured as the load was moved upward by applying a stepped torque at each joint from a stationary state for various angles of θ.

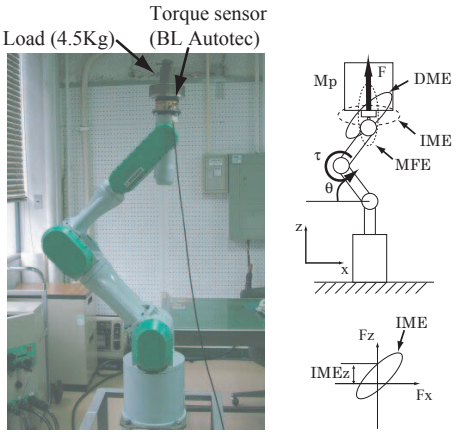

Fig. 9. Experimental setup

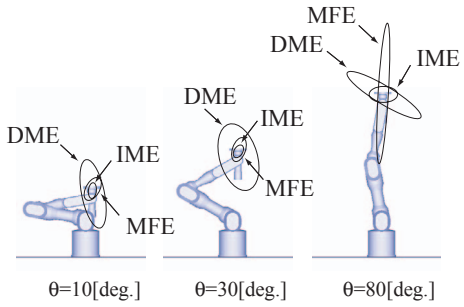

Fig. 10. DME, MFE, and IME for various postures

Figure 11 illustrates the inertia matching index defined by Eq. (26) on the $x-z$ plane. As mentioned above, the inertia matching index evaluates the torque-force transmission efficiency for all directions at a reference point, i.e. a hand position. In order to focus on the actual torque-force transmission efficiency for the upper direction which takes the effect of the nonlinear term F_{bias} into account, we evaluated the magnitude of ellipsoids defined by Eq. (18) from a hand position in the z direction. Figure 12 illustrates the magnitudes of the MFE and IME in the z direction (IMEz in Fig. 9) predicted from the simulations. Since the center of the ellipsoid is translated by the bias term, IMEz does not equal to the length from the center of the IME to the IME. The MFE indicates

the production of an infinite force in the upward direction if the manipulator stretches completely, whereas the IME yields a small transmitted force in the upward direction as the manipulator approaches the straight posture.

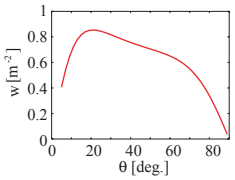

Fig. 11. Inertia matching index for various postures

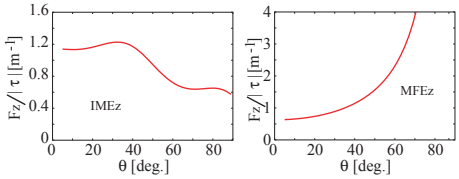

Fig. 12. MFE and IME for various postures

Figure 13 shows the experimental results for the PA-10. The variation in the transmission ratio with posture is almost coincident with that expected by the IME. The joint torque in Fig. 13 is calculated by multiplying the measured output torque around the actuator axis by the gear ratio. Therefore, the transmission ratio is a little smaller than the expected value given by the simulations, which do not consider the transmission efficiency.

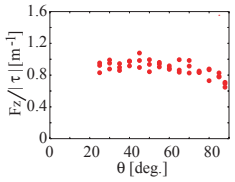

Fig. 13. Measured transmission ratio between joint torque and force applied to the load

The net force and torque required to accelerate the load upward are shown in Fig. 14, where the calculated IME is obtained by subtracting the torque required to support the manipulator and load, and the measured transmission ratio is calculated by subtracting the force imparted by the load in the stationary state.

Figure 14 indicates that there is an optimal posture at which the highest transmission ratio is obtained, as predicted by the IME. Inertia matching between the weight of the load and the manipulator is therefore realized by this posture.

V. Conclusion

The inertia matching ellipsoid was proposed a new index for dynamic performance analysis of a serial link manipulator. The IME provides a measure of the dynamic torque-force transmission efficiency between actuators at joints and a load held by an end-effecter, encompassing a wide range of existing concepts of manipulator performance. The dynamic

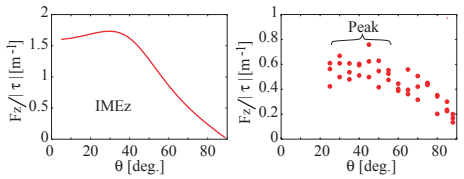

Fig. 14. IMEz and measured transmission ratio with compensation for the weight of the load and the manipulator

manipulability ellipsoid and manipulating-force ellipsoid can both be derived from the IME as limiting forms with respect to the weight of the load. The IME was demonstrated through numerical examples, including the selection of an optimal leg posture for a jumping robot and extension to a free-flying manipulator on a satellite in space. Experiments using a typical serial link manipulator were also performed.

Acknowledgment

This research was supported in part by the 21st Century Center of Excellence Program under the title of “Reconstruction of Social Infrastructure Related to Information Science and Electrical Engineering”, and by the Ministry of Public Management, Home Affairs, Posts and Telecommunications of Japan under the Strategic Information and Communications R&D Promotion Programme (SCOPE).

References

[1] T. Yoshikawa, “Manipulability of robot mechanisms,” *The International Journal of Robotics Research*, vol. 4, no. 2, pp. 3–9, 1985.

[2] R. Koeppe and T. Yoshikawa, “Dynamic manipulability analysis of compliant motion,” in *Proceedings of the IEEE/RSJ International Conference on Intelligent Robots and Systems ’97*, 1997.

[3] T. Yoshikawa, “Dynamic manipulability of robot manipulators,” *Journal of Robotics Systems*, vol. 2, no. 1, pp. 113–124, 1985.

[4] M. T. Rosenstein and R. A. Grupen, “Velocity-dependent dynamic manipulability,” in *Proceedings of the IEEE International Conference on Robotics and Automation*, 2002.

[5] S. L. Chiu, “Task compatibility of manipulator postures,” *The International Journal of Robotics Research*, vol. 7, no. 5, pp. 13–21, 1988.

[6] C. A. Klein and B. E. Blaho, “Dexterity measures for the design and control of kinematically redundant manipulators,” *The International Journal of Robotics Research*, vol. 6, no. 2, pp. 72–83, 1987.

[7] T. J. Graettinger and B. H. Krogh, “The acceleration radius: a grobal performance measure for robotic manipulators,” in *Proceedings of the IEEE/RSJ International Conference on Intelligent Robots and Systems ’88*, vol. 2, 1988, pp. 965–971.

[8] H. Asada, “A geomettrical representation of manipulator dynamics and its application to arm design,” *Journal of Dynamic Systems, Measurement, and Control*, vol. 105, no. 3, pp. 131–135, 1983.

[9] R. Kurazume and T. Hasegawa, “Impedance matching for free flying robots (in japanese),” in *The 20th Annual Conference of the Robotics Society of Japan*, 2002, p. 3J16.

[10] P. Chiacchio, “New dynamic manipulability ellipsoid for redundant manipulators,” *Robotica*, vol. 18, no. 4, pp. 381–387, 2000.

[11] K. Yoshida, H. Nakanishi, H. Ueno, N. Inaba, T. Nishimaki, and M. Oda, “Dynamics, control, and impedance matching for robotic capture of a non-cooperative satellite,” *Advanced Robotics*, vol. 18, no. 2, pp. 175–198, 2004.

[12] J. K. Salisbury, “Active stiffness control of a manipulator in cartesian coordinates,” in *Proc. IEEE Conference on Decision and Control*, 1980, p. 102.

[13] Y. Umetani and K. Yoshida, “Continuous path control of space manipulators mounted on omv,” *Acta Astronautica*, vol. 15, no. 12, pp. 981–986, 1987.

[14] K. Yoshida, R. Kurazume, N. Sashida, and Y. Umetani, "Modeling of collision dynamics for space free-floating links with extended generalized inertia tensor," in *Proc. IEEE Int. Conf. on Robotics and Automation*, 1992, pp. 889–904.